Journal of the European Ceramic Society **17** (1997) 983–994

PII: S0955-2219(96)00198-7
0955-2219/97/$17.00

Microstructural Development during Liquid Phase Sintering of Silicon Carbide Ceramics

L. K. L. Falk

Department of Physics, Chalmers University of Technology, S-412 96 Göteborg, Sweden

(Received 29 April 1996; revised version received 19 September 1996; accepted 23 September 1996)

Abstract

The microstructures of liquid phase sintered α-SiC ceramics have been characterised by analytical electron microscopy including electron energy filtered imaging. The materials were fabricated with different additions of Al_2O_3 and/or Y_2O_3 and densified by pressureless sintering or hot isostatic pressing (HIP). Y, Al-garnet and α-Al_2O_3 partitioned from the liquid phase sintering medium during pressureless sintering leaving only thin intergranular films of residual glass. The formation of α-Al_2O_3 was promoted by the incorporation of Al_2O_3 from the surrounding SiC/Al_2O_3 powder bed. The thickness of analysed Al- and O-rich glassy films at SiC/SiC grain boundaries was estimated to be 1·4–1·5 nm by Fresnel out-of-focus imaging. The crystallisation of Y-, Al-, Si- and O-rich liquids was suppressed during HIP, however, $Y_2Si_2O_7$ partitioned from the liquid phase sintering medium in the absence of Al. The applied high pressure during HIP resulted in a limited decomposition of the α-SiC whereby graphite and SiO_2 formed. © *1997 Elsevier Science Limited.*

1 Introduction

The fabrication of dense SiC ceramics requires a sintering additive because of the extremely low self diffusivities in the strongly covalently bonded α- and β-SiC structures.[1,2] An effective additive promotes densification and creates an atmosphere which inhibits the decomposition of the SiC compound at the high sintering temperature. Different metals and metal oxides and nitrides have been used as sintering aids in previous studies, and proposed reactions during densification have been dependent upon the particular additive and the fabrication process.[2–6]

Additions of metal oxides participate in liquid phase formation at elevated temperatures, and these liquids act as mass transport media during densification.[7–9] The major requirements on the liquid phase sintering medium are that there is a sufficient volume fraction of liquid which exhibits complete wetting of the solid phase, and that the solid phase has an appreciable solubility in the liquid. The transport properties of the liquid phase will be dependent upon its volume fraction and chemistry. These are determined by the particular metal oxide, relevant eutectic temperatures and by densification parameters such as temperature and atmosphere. Densification rate as well as grain growth during liquid phase sintering, and thereby the grain size and shape distributions of the sintered material, may thus be controlled through the fabrication parameters. The improved strength of SiC ceramics which in some cases has been obtained by liquid phase sintering has been attributed to reduced grain growth; these microstructures did not contain the very large SiC grains which generally are present in solid-state sintered SiC ceramics and act as stress concentrators.[6] The mechanical and chemical properties of the liquid phase sintered SiC ceramic will, however, also be strongly affected by the intergranular microstructure. This structure is determined by the phase relationships in the particular system as well as by the temperature/time programme during densification. A number of liquid phase sintered ceramics, e.g. Si_3N_4-based ceramics, have been reported to contain a continuous intergranular glassy phase which is the residue of the liquid phase sintering medium.[10,11] This glass softens at increased temperatures and has in general a negative effect on high-temperature mechanical and chemical properties.[9,10]

Densification of SiC ceramics has generally required high sintering temperatures (around 2000°C and above) and high pressures have frequently been applied in order to obtain a fully dense material. Pressureless sintering of SiC was first carried out with smaller amounts of B and C as

sintering aids.[4] Recent work has shown that it is possible to pressureless sinter SiC with additions of Al_2O_3 and Y_2O_3, and it was also demonstrated that these additives makes it possible to reduce the sintering temperature to well below 2000°C.[5,6,12]

This paper focuses on the development of microstructure during liquid phase sintering of α-SiC ceramics with different additions of Al_2O_3 and/or Y_2O_3. The metal oxides were added either as powders or as colloidal sols. It has been demonstrated that the use of colloidal sols as precursors to metal oxide sintering aids may promote fabrication of liquid phase sintered ceramics with improved homogeneity.[12,13] It may also be possible to reduce the amount of additives due to the improved dispersion. The densification of the α-SiC ceramics was carried out either by pressureless sintering in a protective powder bed or by hot isostatic pressing (HIP) using the glass encapsulation technique.

2 Experimental Procedure

2.1 Experimental materials

The experimental α-SiC ceramics were fabricated with different additions of Al_2O_3 and/or Y_2O_3, see Table 1. Some of the green bodies had an Y_2O_3/Al_2O_3 ratio corresponding to that of the Y, Al-garnet, 5 $Al_2O_3 \cdot 3Y_2O_3$. The oxides were added either as powders (Al_2O_3, AKP30, Sumitomo; Y_2O_3, Fine, H.C. Starck) or as colloidal sols (Nyacol Inc), and the α-SiC starting powder (UF 15, Lonza-Werke) had the 6H polytype. The oxygen content of the SiC starting powder corresponded to 2·1 wt% SiO_2. Green bodies were formed by slip casting when the metal oxides were added as powders, and by freeze granulation and subsequent pressing when the colloidal sols were used as precursors to the metal oxides. Detailed descriptions of the processing and densification procedures, and data on some physical properties, have been published previously.[12]

Pressureless sintering was carried out in a SiC/Al_2O_3 powder bed in an Ar atmosphere at 1880°C for 2 or 4 h, Table 1. Some of the green bodies were held at 1600°C for 1 h before the temperature was increased to the final sintering temperature. The aim of this heat treatment was to control the amount of surface silica present on the SiC powder particles. One green body formed with 1·29 wt% Al_2O_3 together with 1·71 wt% Y_2O_3 was characterised after heat treatment at 1600°C. Hot isostatic pressing (HIP) was carried out at 1800°C for 1 or 2 h under a pressure of 160 MPa using the AC Cerama proprietary glass encapsulation technique. The green bodies were heat treated in Ar at 1400°C for 4 h prior to glass encapsulation.

2.2 Microanalysis

2.2.1 Instrumentation

The microstructures were characterised by analytical scanning and transmission electron microscopy (SEM/TEM/STEM/EDX) and X-ray diffractometry. Polished sections were imaged by back-scattered and secondary electrons in a CamScan 4S-80DV instrument equipped with an EDX detector with an open window capability for light element detection and a Link eXL EDX system for quantitative elemental analysis. The detailed characterization of the microstructures was carried out in a JEOL 2000-FX TEM/STEM/SEM instrument and a Philips CM200 SuperTwin TEM with a field emission gun (FEG). The FEG TEM is equipped with a post-column Gatan imaging filter (GIF) and a Link Isis EDX system with a super-ATW window in front of the detector which

Table 1. The experimental materials in the present investigation. The phase compositions were determined by X-ray diffractometry and electron diffraction in the TEM

Specimen number/oxide additives	*Densification*	*Phase composition*
Metal oxide powders	*Pressureless sintering*	
A 3 wt% Y_2O_3	1 h at 1600°C, 4 h at 1880°C	6H, 4H, YAG, α
B 1·3 wt% Al_2O_3 + 1·7 wt% Y_2O_3*	1 h at 1600°C, 4 h at 1880°C	6H, 4H, YAG, α
C 2 wt% Al_2O_3 + 1 wt% Y_2O_3	2 and 4 h at 1880°C	6H, 4H, YAG, α
D 4 wt% Al_2O_3 + 2 wt% Y_2O_3	2 and 4 h at 1880°C	6H, 4H, YAG, α
Colloidal sols	*Pressureless sintering*	
E 2 wt% Al_2O_3 + 1 wt% Y_2O_3	1 h at 1600°C, 4 h at 1880°C	6H, 4H, YAG, α
Colloidal sols	*Hot isostatic pressing (HIP)*	
F 1 wt% Y_2O_3	1 h at 1800°C, 160 MPa	6H, 4H, YSO, G, C
G 1·3 wt% Al_2O_3 + 1·7 wt% Y_2O_3*	2 h at 1800°C, 160 MPa	6H, 4H, G, C

Legend: 6H, 4H = α-SiC polytypes; YAG = $5Al_2O_3 \cdot 3Y_2O_3$; α = α-Al_2O_3; YSO = α-$Y_2Si_2O_7$; G = glass pockets; C = graphite.
*Y, Al-garnet composition: $5Al_2O_3 \cdot 3Y_2O_3$.

allows light element analysis. The SiC samples were sufficiently conducting under the electron beam in both SEM and TEM and did not require any coating for imaging and analysis. The thin foils for TEM were prepared by standard techniques; i.e. grinding, polishing and dimpling to a thickness of around 40 μm followed by ion beam thinning. Sputtering was carried out by 4 kV Ar ions at an incidence angle of 20°.

2.2.2 Analytical techniques

Phase identification in the TEM was carried out by selected area electron diffraction and micro/convergent beam diffraction together with fine probe EDX analysis. The probe size (FWHM) used for EDX analysis of intergranular regions in the FEG TEM was nominally around 1 nm. Diffuse dark field imaging was used to reveal amorphous pockets and grain boundary films in the microstructures.

The presence of SiC grain boundary films was also indirectly determined by out-of-focus bright field imaging of edge-on grain boundaries. Out-of-focus images will include a pair of bright or dark lines, Fresnel fringes, delineating the grain boundary if an intergranular film is present. The spacing of the fringes decreases when the amount of defocus is decreased, and the fringe contrast is reversed when going through the Gaussian focus in a through focus series. The formation of the Fresnel fringes is caused by a phase shift which is proportional to the difference in mean inner potential.[14]

The thickness of amorphous SiC grain boundary films was estimated from plots of Fresnel fringe spacing versus defocus in digital through focus series. The fringe spacing (W) is dependent upon grain boundary film thickness (t) according to the relationship

$$W = t - (3\lambda\Delta f)^{1/2} \quad (1)$$

where λ is the electron wavelength and Δf is the defocus.[15] The intersection of plots of over and under focus series extrapolated to zero defocus represents the grain boundary film thickness.[14]

Electron energy filtered images were recorded using the C K, O K, and Al $L_{2,3}$ edges in the electron energy loss spectrum (EELS). One post-edge and two pre-edge images were acquired using a slit width of 30 eV for C and 50 eV for O. A background image was estimated from the two pre-edge images and subtracted from the post-edge image. This procedure gave maps of the C and O edge intensities versus position in the microstructure. The Al distributions were imaged by taking the ratio of a post-edge and a pre-edge image using a slit width of 20 eV.

3 Results

3.1 Microstructure of pressureless sintered materials

The pressureless sintered materials showed the same general microstructure independent of starting powder composition and time at sintering temperature, Table 1. Two crystalline intergranular phases, α-Al_2O_3 and $5Al_2O_3{\cdot}3Y_2O_3$ (Y, Al-garnet), were identified by electron diffraction and EDX in the TEM. These two phases were present in all pressureless sintered materials, i.e. also in the material formed without the addition of Al_2O_3 and in the material formed with an Y_2O_3/Al_2O_3 ratio corresponding to that of the Y, Al-garnet.

The distribution of the two crystalline intergranular phases was clearly revealed in the SEM, see Fig. 1. Images obtained by secondary electrons showed bright contrast from the α-Al_2O_3. This type of contrast difference between the SiC and the Al_2O_3 is due to the different electrical properties of the two phases; SiC is a better conductor than Al_2O_3. The α-Al_2O_3 formed larger pockets in the microstructure; some of them were of the same size as the SiC grains. Imaging by back-scattered

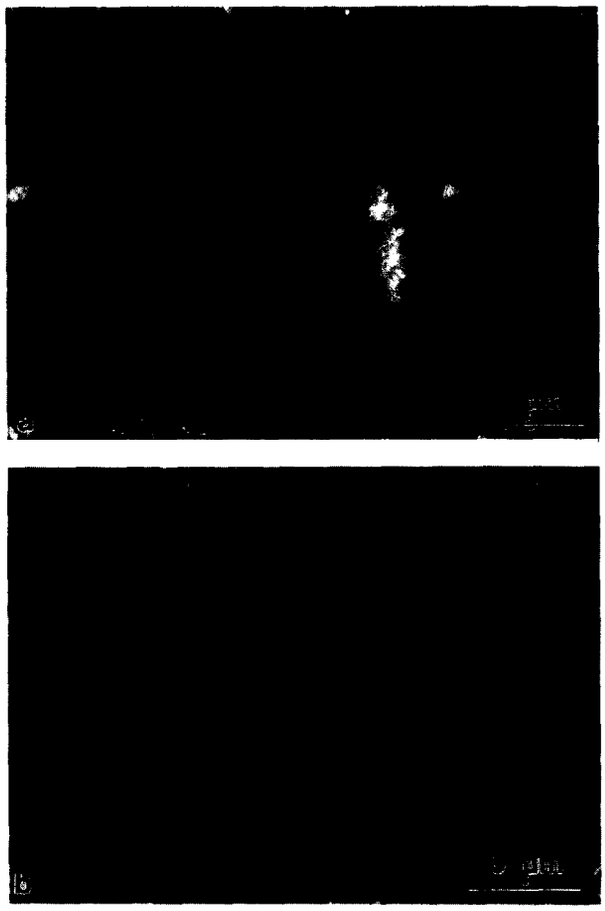

Fig. 1. Polished section of a pressureless sintered material imaged in the SEM by (a) secondary electrons and (b) back-scattered electrons. These images show the distributions of α-Al_2O_3 (a) and Y, Al-garnet (b). The materials contained also some porosity (arrowed).

electrons showed the distribution of the Y, Al-garnet. This phase formed smaller pockets in the microstructure, and imaging at lower magnifications clearly showed that the distribution of Y was inhomogeneous. This was also the case when sols had been used as precursors to the metal oxide additives.

Centred dark field imaging and electron diffraction in the TEM showed that the Y, Al-garnet was present with the same crystallographic orientation over larger areas, Fig. 2. The pockets were, however, not fully crystallised; thin amorphous films separated the garnet from the surrounding SiC grains, Fig. 2. Glassy films were present also at α-Al_2O_3/SiC boundaries. Polyphase pockets containing grains of both α-Al_2O_3 and Y, Al-garnet could be observed only in a few cases.

The SiC grain size in the areas containing the crystalline intergranular phases was typically around 1–2 μm and the apparent grain shape varied. Smaller SiC grains inside larger pockets of Y, Al-garnet, as well as some SiC grains facing such pockets, often had a rounded shape, Fig. 2. However, faceted SiC grains were also observed in these areas. A limited number of significantly larger grains with an irregular shape and a size of up to around 5 μm were also present. X-ray diffraction indicated that there was a limited

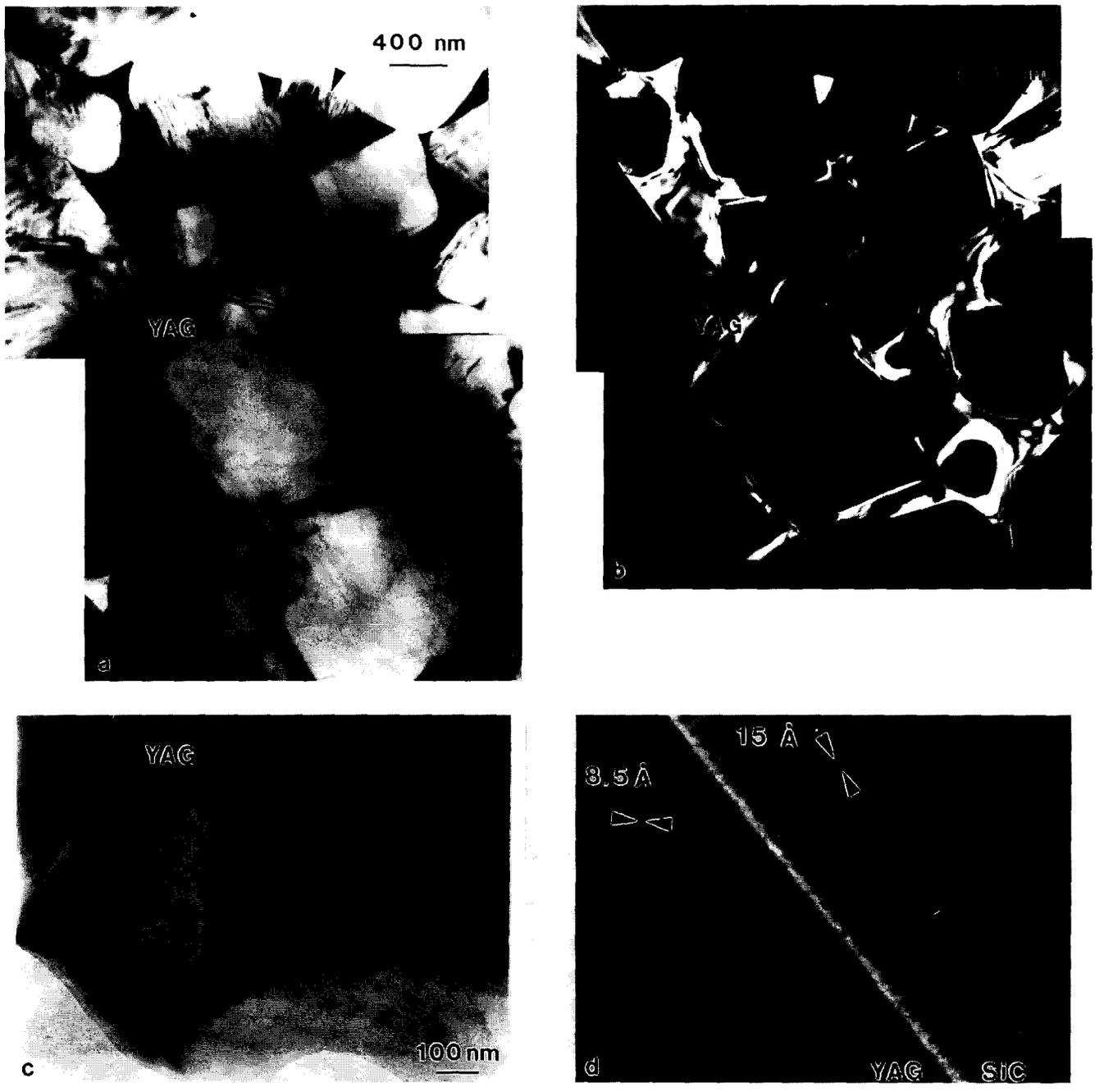

Fig. 2. Pockets of Y, Al-garnet (YAG) in a pressureless sintered material (a), (b) and (c). The centred dark field image in (b) was formed with a {321} reflection from the YAG and shows the same area as (a). Some of the α-SiC grains had a faulted structure (arrowed). TEM lattice fringe image (d) showing the presence of a grain boundary film at a YAG/α-SiC boundary. The lattice fringes correspond to the {110} planes in the YAG and to the (0001) planes in the α-SiC 6H polytype.

transformation from the 6H to the 4H polytype of α-SiC in all samples, Table 1, which would be consistent with the observed faulted structure in a number of the α-SiC grains, Figs 2–4. Faceted as well as smaller grains inside larger pockets did in general have the 6H polytype.

Thin amorphous films were always present at SiC/SiC grain boundaries in the dense areas, Figs 3 and 5. Electron energy filtered imaging and fine probe EDX analysis showed that these films were rich in Al and O, and contained less C than the surrounding SiC grains, see Fig. 3. Films merging into smaller glass pockets containing Y and impurities (e.g. Ca) contained also these cations. EDX profiles across edge-on grain boundaries did not reveal any incorporation of other cations or O into the SiC structure. The thickness of Al- and O-containing glassy grain boundary films merging into pockets containing the Y, Al-garnet was estimated to 1·4 to 1·5 nm from through focus series, see Fig. 5.

SEM of polished sections revealed a certain amount of porosity in the pressureless sintered materials, see Fig. 1. Grinding and polishing may introduce pores and affect the apparent porosity of a ceramic. However, TEM clearly showed that there was a third type of microstructural region in these materials, Fig. 4. Interparticle contact areas in these partially sintered regions contained thin amorphous films. The pore walls were also covered by amorphous films of different thicknesses and morphologies, and these films were rich in Si and O and frequently also contained Al. The SiC grain size in the partially sintered regions was typically less than 1 μm. The apparent porosity was not reduced when the metal oxide starting powders were replaced by colloidal sols.

3.2 Microstructures of hot isostatically pressed materials

The chemistry and structure of the intergranular regions in the two materials densified by HIP did clearly reflect the different starting powder compositions, see Table 1. The addition of colloidal sols corresponding to a metal oxide addition of 3 wt% with the same Al_2O_3/Y_2O_3 ratio as that of the Y, Al-garnet did not result in the formation of secondary crystalline phases. Thin amorphous intergranular films merged into larger glass pockets at multi grain junctions, Fig. 6. Fine probe EDX analysis together with electron energy filtered imaging showed that the pockets as well as the grain boundary films were rich in Si, Al, Y and O, but depleted in C, Fig. 7. The composition of the glass pockets varied; some pockets had an Y/Al ratio close to that of the Y, Al-garnet while other pockets had a significantly higher relative Al content and contained also a larger amount of Si.

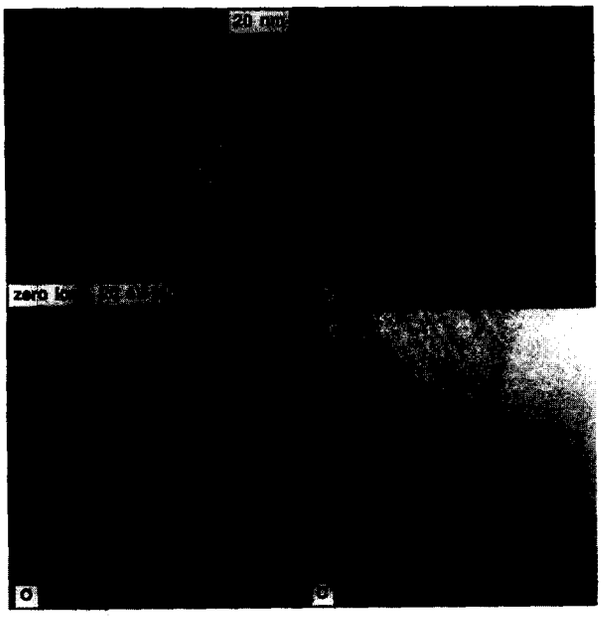

Fig. 3. Electron spectroscopic images of a pressureless sintered material. An Y-, Al- and O-rich glassy phase is present as thin intergranular films merging into a small pocket at a triple junction. The faulted structure of some α-SiC grains is clearly shown in the zero loss image.

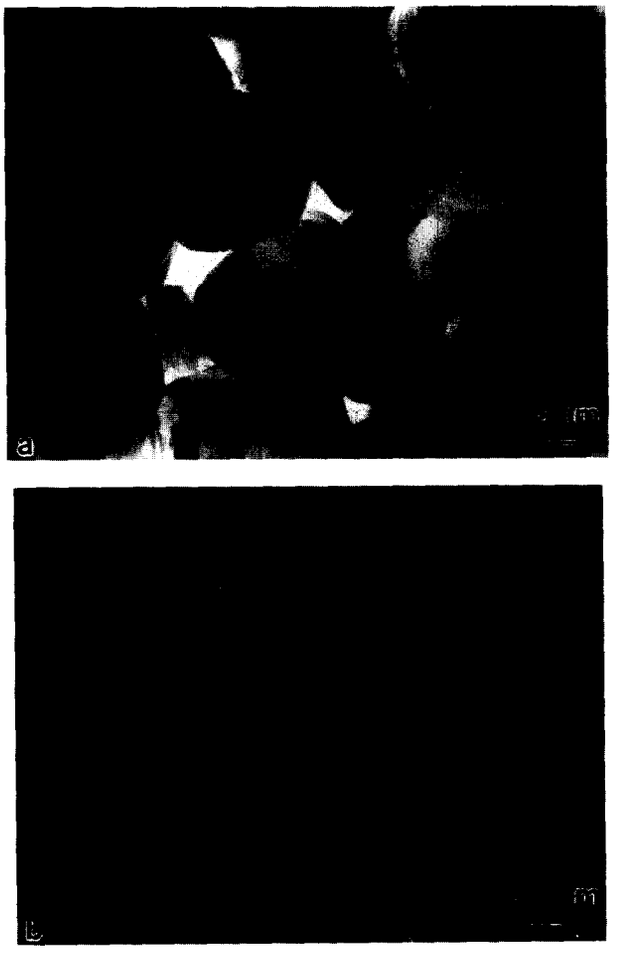

Fig. 4. Partially sintered areas in a pressureless sintered material. Centred dark field imaging using diffuse scattered electrons (b) showed that interparticle contact areas contained thin glassy films and that the particles were covered with an amorphous phase (arrowed).

Two types of intergranular region formed during HIP when only a small amount of Y_2O_3 sol (corresponding to 1 wt% Y_2O_3) was added. Pockets at multi grain junctions contained either α-$Y_2Si_2O_7$ or an Si- and O-rich glassy phase, Fig. 8. The α-$Y_2Si_2O_7$ was separated from surrounding SiC grains by thin amorphous films, and the SiC/SiC grain boundaries contained thin glassy films also in this material.

X-ray diffraction indicated that there was a transformation from the 6H to the 4H polytype also in the HIP:ed α-SiC materials, and a number of the α-SiC grains showed a faulted structure, Figs 6 and 8. The SiC grain size and shape distributions in the material containing the Y- and Al-rich glass were similar to those in the dense areas of the pressureless sintered materials, while the smaller Y_2O_3 addition resulted in a microstructure with an irregular grain shape and a limited variation in grain size. Analysed SiC grains did not contain any detectable amounts of dissolved elements.

The hot isostatically pressed materials contained microstructural features which were not observed in the pressureless sintered materials. Electron diffraction and EDX showed that

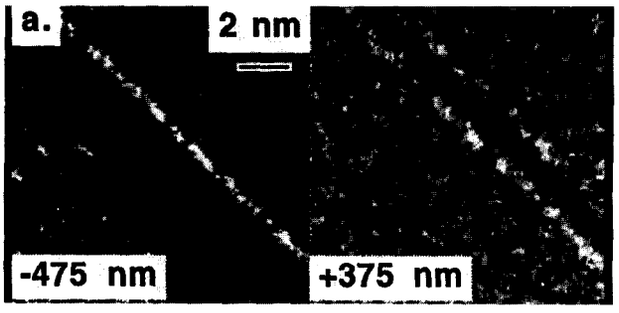

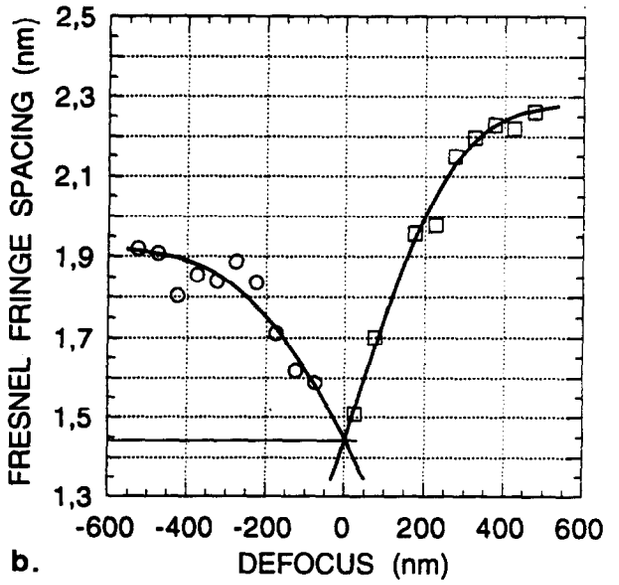

Fig. 5. Over- and underfocused images of a SiC/SiC grain boundary showing (a) Fresnel fringe contrast, (b) Fresnel fringe spacing as function of defocus. The film thickness was estimated to be 1·4–1·5 nm.

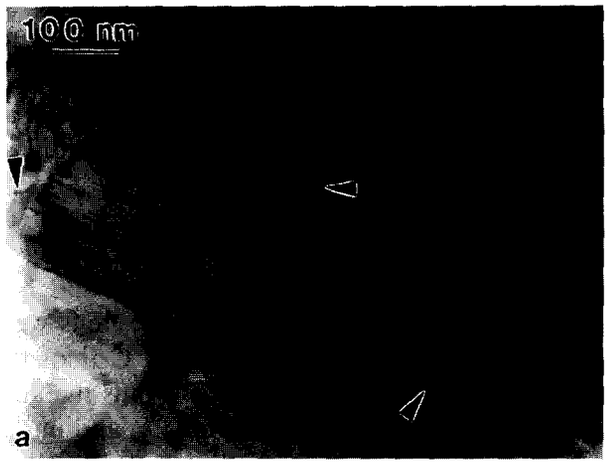

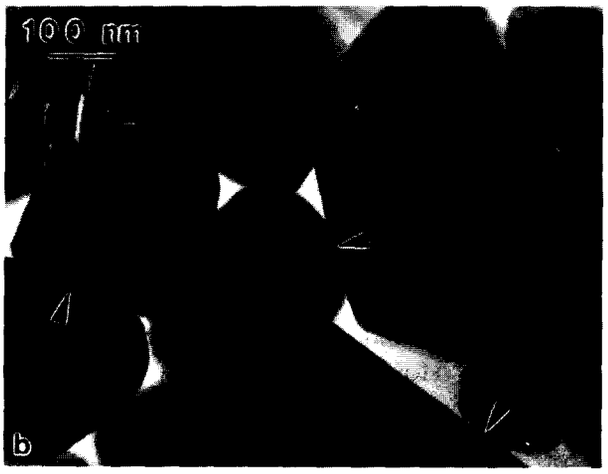

Fig. 6. The general microstructure of the material HIP:ed with 1·3 wt% Al_2O_3 + 1·7 wt% Y_2O_3. The intergranular glassy phase is arrowed in the TEM bright field image (a) and the centered dark field image formed by diffuse scattered electrons (b). The faulted structure of some α-SiC grains is shown in (a).

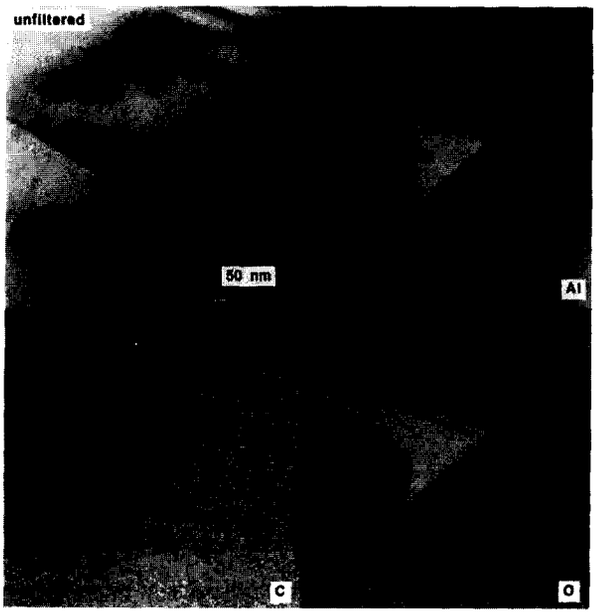

Fig. 7. Electron spectroscopic imaging of amorphous grain boundary films merging into a glassy pocket in the material HIP:ed with 1·3 wt% Al_2O_3 + 1·7 wt% Y_2O_3.

graphite had formed during HIP, Figs 9 and 10. The graphite was present both in smaller pockets at multi grain junctions and in comparatively large volumes between SiC grains. The SiC grains surrounding the larger graphite-containing volumes had an irregular shape due to cavity formation at grain facets, Fig. 10. The presence of smaller amounts of graphite in glassy pockets was often associated with voids in the glass. The crystallinity of the graphite was sensitive to the electron beam; these features became amorphous under prolonged exposure.

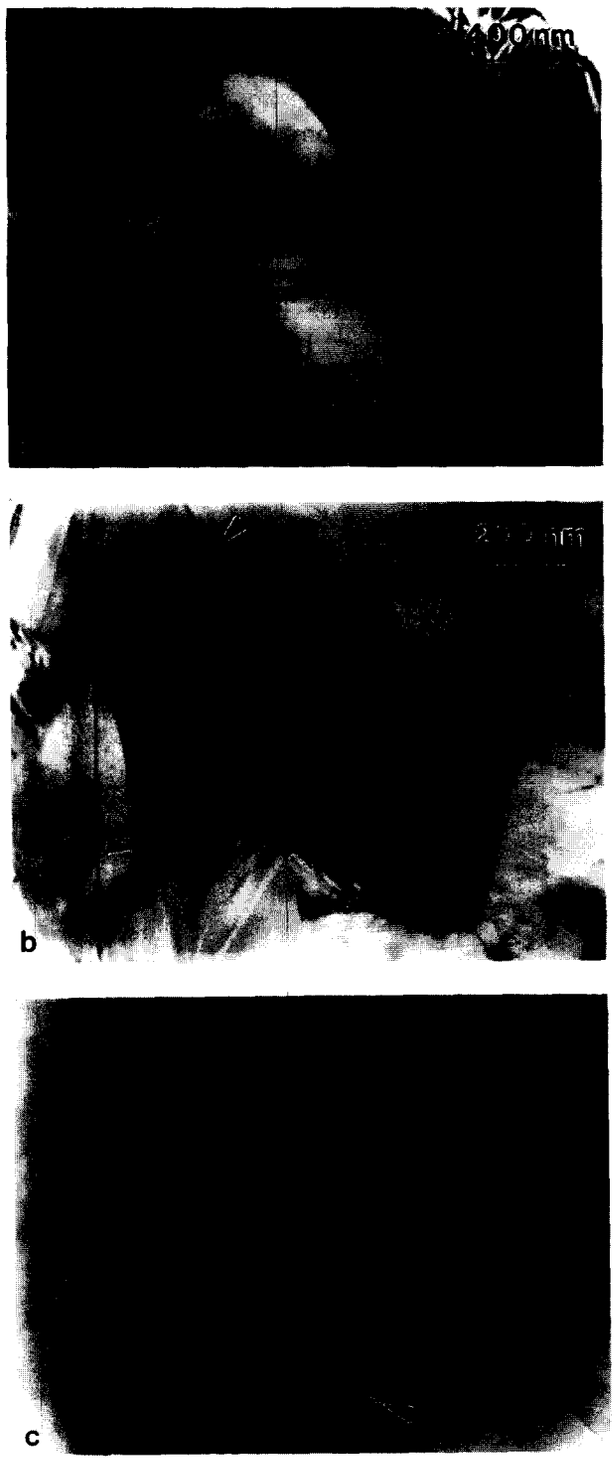

Fig. 8. The general microstructure of the material HIP:ed with 1 wt% Y_2O_3. The faulted structure of some α-SiC grains is shown in (a)–(c). Intergranular pockets contained either α-$Y_2Si_2O_7$, arrowed in (b), or an Si- and O-rich glass, arrowed in (c).

3.3 Heat treated green bodies

The heat treatment at 1600°C for 1 h of the green body formed with 1·29 wt% Al_2O_3 and 1·71 wt% Y_2O_3 resulted in a limited densification. Contact areas between SiC powder particles created during this initial sintering stage contained amorphous films, and powder particle surfaces exposed to pores were generally covered by silica-rich glassy films. A limited formation of smaller Y- and Al-rich pockets was observed in dense areas, Fig. 11.

4 Discussion

4.1 Densification

The characterisation of the heat treated green body showed that bonding of the SiC starting powder particles was the first stage in the densification process. The contact areas contained thin amorphous films which implies that the initial step in the sintering of the SiC particles was a reaction

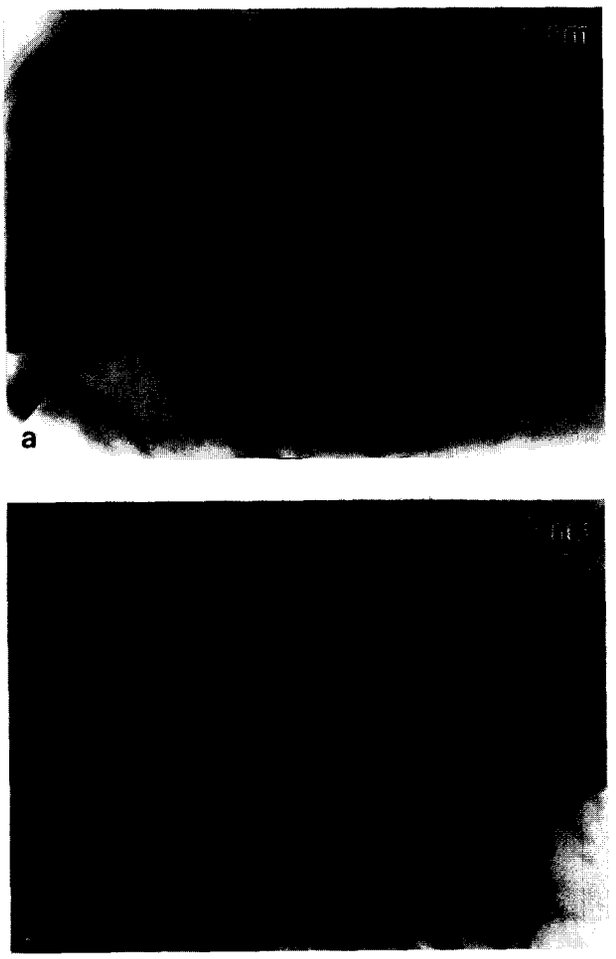

Fig. 9. Graphite formation (arrowed) in the material HIP:ed with (a) 1·3 wt% Al_2O_3 + 1·7 wt% Y_2O_3 and (b) 1 wt% Y_2O_3.

between the native surface silica layers. This reaction started at a comparatively low temperature and prior to any appreciable liquid phase formation. Joining of the SiC starting powder particles resulted in an early formation of a SiC network and parts of this network were retained as the porous regions in the pressureless sintered materials. Liquid phases which formed at higher temperatures subsequently filled the voids in the open SiC structure, and the interparticle silica layers would also become liquid (SiO_2 melts at 1726°C).[16] However, these small amounts of metal oxide additives required an applied high pressure for full infiltration and densification.

The microstructures of the pressureless sintered materials and the material hot isostatically pressed with Al_2O_3 and Y_2O_3 show that these metal oxides reacted during the densification process whereby a liquid phase sintering medium was formed. The lowest eutectic temperature in the Al_2O_3/Y_2O_3 system is at 1760°C and has a composition of around 60 wt% Al_2O_3.[17] The presence of the surface silica on the SiC starting powder particles clearly reduces the eutectic temperatures, see Fig. 12; the lowest eutectic temperature in the Al_2O_3–Y_2O_3–SiO_2 system is at 1345°C in the $Y_2O_3{\cdot}2SiO_2$–SiO_2–$3Al_2O_3{\cdot}2SiO_2$ compatibility triangle.[18] A liquid phase formation involving the oxide additives and some of the surface silica present on the SiC starting powder particles may thus take place during heating to the densification temperature, and this was also implied by the presence of a few Y- and Al-rich pockets in the green body heat treated at 1600°C, Fig. 11.

The presence of α-Al_2O_3 in all the pressureless sintered materials, also in the material formed without the addition of Al_2O_3 and in the one formed with an Al_2O_3/Y_2O_3 ratio corresponding to that of the Y, Al-garnet, shows that there was a transport of Al_2O_3 from the surrounding SiC/Al_2O_3 powder bed into the body during sintering. The presence of Al in the Si- and O-rich layers on particles in partially sintered, porous, regions implies that this transport was associated with vapour phase reactions. This is consistent with previous observations.[19] It was suggested that the Al_2O_3 in the powder bed may be decomposed by

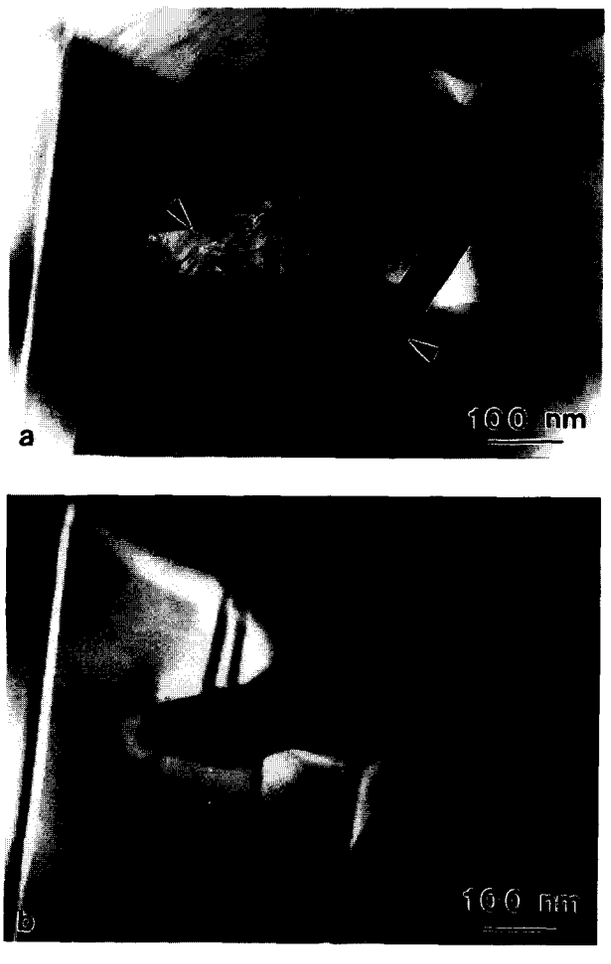

Fig. 10. Graphite-containing cavity (arrowed) at a SiC grain facet. (a) Bright field TEM image and (b) centred dark field image clearly revealing the shape of the SiC grain.

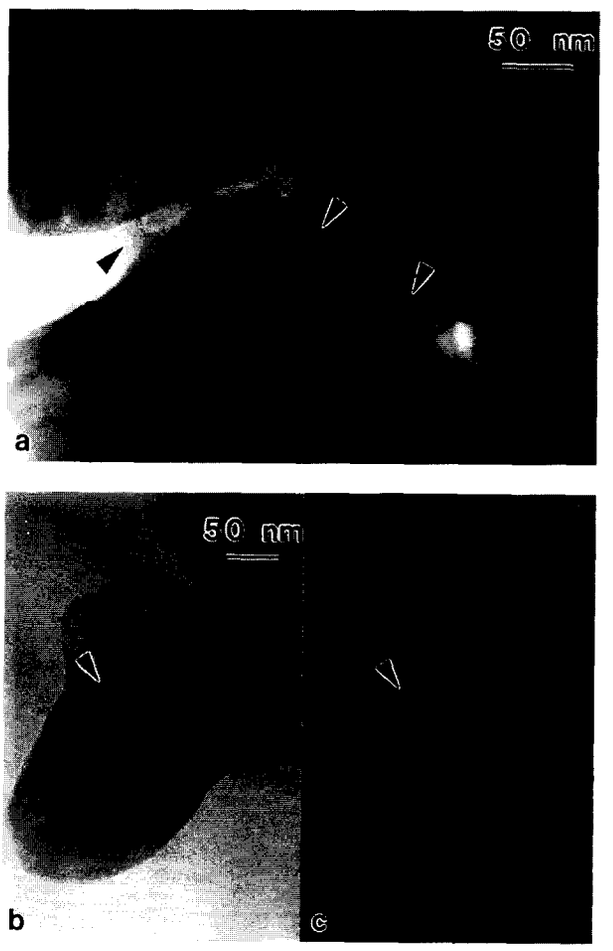

Fig. 11. Green body formed with 1·3 wt% Al_2O_3 + 1·7 wt% Y_2O_3 after heat treatment at 1600°C for 1 h. SiC particles are bonded by an amorphous phase (arrowed) (a). Smaller pockets of Y-, Al- and O-rich glass (arrowed) had formed locally; (b) TEM bright field image and (c) centred dark field image formed by diffuse scattered electrons.

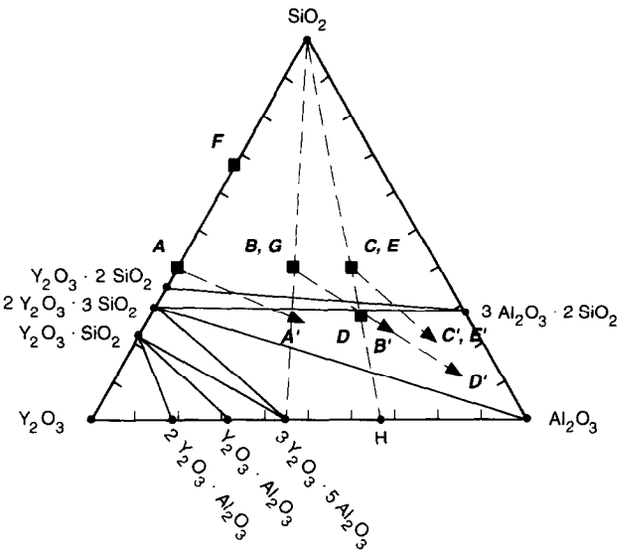

Fig. 12. The Al_2O_3–Y_2O_3–SiO_2 phase diagram in wt% after Ref. 18. Point H represents an Al_2O_3:Y_2O_3 weight ratio of 2:1. Specimen numbers A–E refer to the processing conditions given in Table 1. A'–E' indicate the effect of the Al_2O_3 uptake during pressureless sintering.

the C which is generally present in the surrounding environment during pressureless sintering. Thermodynamical considerations indicated that gaseous AlO and Al_2O would form during this decomposition, and that their partial pressures would be sufficient to cause the observed Al_2O_3 formation in the SiC body.[19]

The overall oxide compositions of the different materials are shown in the phase diagram in Fig. 12. It may, however, be expected that grinding and powder mixing increased the SiO_2 contents of the green bodies further. The effect of the Al_2O_3 uptake during pressureless sintering of compositions A–E in Table 1 is indicated in the phase diagram. The coexistence of Y, Al-garnet and α-Al_2O_3 in all pressureless sintered materials implies that the garnet partitioned from the liquid at high temperature.

The lowest eutectic temperature in the Y_2O_3–SiO_2 system is in the SiO_2-rich part at 1660°C;[20] liquid phase formation would thus start at a higher temperature in the absence of Al_2O_3. The co-existence of α-$Y_2Si_2O_7$ and pockets of an Si–O-rich glass in the material hot isostatically pressed with 1 wt% Y_2O_3 implies that liquid silica was present in addition to the Y_2O_3–SiO_2 liquid during densification; this is consistent with SiO_2 melting at 1726°C.[16] This two-phase intergranular microstructure shows that this small Y_2O_3 addition was not sufficient to incorporate the surface silica on the SiC starting powder particles into secondary crystalline phases. If all of the added Y_2O_3 produced α-$Y_2Si_2O_7$, a silica content corresponding to 0·54 wt% SiO_2 was consumed in this reaction. Hence, this is consistent with the significantly higher oxygen content of the green body as shown in Fig. 12.

4.2 Crystallisation of intergranular volumes

Partitioning of the cubic Y, Al-garnet from the liquid phase sintering medium during pressureless sintering resulted in neighbouring pockets with the same crystallographic orientation. This suggests that the crystallisation involved comparatively few nucleation sites and that the garnet grew in a three-dimensional intergranular network. Such intergranular morphology has also been observed when the cubic Y, Al-garnet forms in β-sialons and when cubic Y_2O_3-stabilised ZrO_2 partitions from the oxynitride liquid phase sintering medium during densification of Si_3N_4/ZrO_2 ceramics.[7,21]

Formation of secondary crystalline phases did not result in full crystallisation of the intergranular regions; thin glassy films separated these phases from surrounding SiC grains. The partitioning of secondary crystalline phases from the liquid phase sintering medium may introduce a change in composition of the residue which results in a good glass former. Y was absent in SiC/SiC grain boundary films merging into pockets containing the Y, Al-garnet. This implies that the crystallisation of the Y, Al-garnet depleted the remaining liquid of Y and hence shifted the composition of the residual liquid/glass phase towards the Al_2O_3–$3Al_2O_3{\cdot}2SiO_2$ or the SiO_2–$3Al_2O_3{\cdot}SiO_2$ tie line, see Fig. 12.

The retention of a thin amorphous grain boundary film may not only be caused by its chemistry. Theoretical modelling based upon continuum approaches considering either interfacial energies or the force balance normal to the grain boundary postulate that there is an equilibrium thickness of the amorphous grain boundary film.[22] This would thus present an obstacle to full crystallisation of the intergranular microstructure in liquid phase sintered SiC ceramics, and explain the presence of thin glassy films also at SiC/SiC grain boundaries. The equilibrium film thickness is the result of competing interactions; an attractive van der Waals interaction between the grains on each side of the boundary and a repulsive interaction due to film structure. These models also indicate that thin intergranular liquid/glass films can support stresses normal to the boundary, and that the stable film thickness is strongly dependent upon the dielectric properties of the adjacent grains.[22,23]

The Al_2O_3 and Y_2O_3-rich liquid was retained as a residual intergranular glassy phase after HIP despite that a number of the analysed glass pockets had an Y/Al ratio close to that of the Y, Al-garnet. This indicates that factors other than composition

would also determine the degree of equilibrium crystallisation of intergranular liquid and glass phases and this lends support to theoretical work.[22-25] A different stress/strain state in the body due to the applied high pressure may affect the formation of secondary crystalline phases; liquid and glass phases support hydrostatical stresses which present an obstacle to their crystallisation.[24,25] Theoretical and experimental work has shown that under given conditions there is a critical volume of the pocket for crystallisation to be energetically favourable.[24,26] The temperature/time programme, e.g. the degree of supercooling and the cooling rate, are other factors affecting crystallisation.[25]

4.3 SiC grain morphology

Larger pockets of Y,N-garnet often contained SiC grains with small and rounded sections, and the SiC grains surrounding such pockets had either a rounded or a faceted shape. This implies that a solution/reprecipitation process occurred during densification; SiC grains with smaller and/or rounded sections would be under dissolution in the liquid phase sintering medium while grains with faceted sections would be growing. This solution/reprecipitation process did not affect the polytype content in any obvious way. Electron diffraction from grains with faceted sections showed that these grains had the α-SiC 6H polytype. The faceted shape is, hence, reflecting the hexagonal crystal structure of the α-SiC. This is similar to growth of β-Si_3N_4 and β-sialon grains in isotropic liquid phase environments; these grains also develop a prismatic shape which reflects their hexagonal lattice.[11] The proposed solution/reprecipitation process would give a certain contribution to the densification of the SiC ceramics. Work on Si_3N_4 ceramics formed with different types of metal oxide additives has, however, shown that the diffusion through Y-containing oxynitride liquids is slow and therefore only gives a smaller contribution to the overall densification.[8]

The proposed solution/reprecipitation did not result in any detectable incorporation of Y, Al or O into the α-SiC 6H structure. This is in contrast to previous work on SiC liquid phase sintered with additions of an Y, Al-garnet powder. Those materials were sintered at a slightly higher temperature (1950°C), and the α-SiC 6H grains had a core/rim structure where the rim contained smaller amounts of dissolved Y, Al and O.[27]

The transformation of the α-SiC 6H to the 4H polytype during densification seemed to occur inside the SiC grains. A similar behaviour has been observed previously during β to α transformation in polycrystalline SiC; 6H formed from the β-SiC 3C structure and was subsequently transformed to the 4H polytype.[28] These transformations were explained in terms of dislocation reactions. The observed 6H to 4H transformation in the present materials would, hence, be affected by local stress/strain states in the body during densification.

4.4 Formation of graphite during HIP

Densification by HIP proceeds in a closed system when the glass encapsulation technique is used, and reactions with the environment are, hence, eliminated. This fabrication technique would therefore enable a more accurate control of phase and elemental contents through choice of starting powder composition and process parameters, and thereby also result in a more homogeneous material. However, the presence of graphite and SiC grain cavities in the HIP:ed materials implies that smaller amounts of Al_2O_3 and Y_2O_3 (3 wt% and less) are not sufficient to suppress the decomposition of the SiC during HIP.

A decomposition of the SiC ceramic can be expressed in terms of oxidation reactions according to proposed models.[19,29] Reactions for the decomposition of SiC by a metal oxide were obtained by subtracting the metal oxide formation reaction from the relevant SiC oxidation reaction in the particular temperature interval. The oxidation reactions with the lowest change in free energy at temperatures around 1800°C are:[19,29]

$$SiC + O_2 \rightarrow SiO_2(s,l) + C\ (s) \quad T < 1527°C \tag{2}$$

$$2/3\,SiC + O_2 \rightarrow 2/3\,SiO_2\ (s,l) + 2/3\,CO \quad 1527°C < T < 1802°C \tag{3}$$

$$SiC + O_2 \rightarrow SiO\ (g) + CO \quad 1802°C < T < 2227°C \tag{4}$$

This indicates that reaction (3) or (4) would be responsible for any decomposition of SiC during HIP at 1800°C; however, the presence of graphite in the HIP:ed materials strongly suggests that reaction (2) takes place.

The effect of high pressures on relevant Ellingham diagrams has previously been established in order to analyse the sintering behaviour of Si_3N_4 ceramics under different conditions.[30,31] Special attention was paid to the stability of impurity C. This work showed that the equilibrium point between reactions (2) and (3) above moves to higher temperatures when the total pressure is increased and that C becomes increasingly more stable with increased pressure. The results indicate that the transition point between reactions (2) and

(3) is at around 1900°C at 60 MPa and at around 2100°C at 200 MPa total applied pressure.[31] This means that reaction (2) above is the oxidation reaction with the lowest change in free energy at 1800°C under an applied pressure of 160 MPa, i.e. under the applied HIP conditions.

Subtraction of the metal oxide formation reaction

$$4/3\ M + O_2 \rightarrow 2/3\ M_2O_3 \qquad (5)$$

where M is Al or Y, from the oxidation reaction (2) results in the following decomposition reaction:

$$SiC + 2/3\ M_2O_3 \rightarrow SiO_2 + 4/3\ M + C \qquad (6)$$

The decomposition (6) is hence proposed as the likely reaction for the observed formation of graphite during HIP of these liquid phase sintered SiC ceramics. This reaction would also result in an increased volume fraction of more silica-rich phases.

5 Conclusions

(a) The inherent surface silica present on the SiC starting powder particles promotes the initial sintering of the SiC green body.

(b) The α-SiC undergoes a solution/reprecipitation process via Y-, Al-, Si-, O-rich liquid phases.

(c) Some of the Al_2O_3 present in a SiC/Al_2O_3 powder bed is incorporated into the SiC compact through vapour phase reactions during pressureless sintering. This promotes the formation of α-Al_2O_3 pockets in the SiC microstructure.

(d) The applied high pressure during HIP of SiC powder compacts containing smaller additions of Al_2O_3 and/or Y_2O_3 cause a decomposition of the SiC resulting in the formation of graphite and SiO_2. It is suggested that the high pressure also affects the crystallisation behaviour of Y-, Al, O-, Si-containing intergranular regions.

(e) Smaller additions of Al_2O_3 and/or Y_2O_3 result in an inhomogeneous intergranular microstructure. The local chemistry will determine the structure and composition of the secondary phases.

(f) Thin intergranular films of residual glass are present throughout the microstructure also when secondary crystalline phases partition from the liquid phase sintering medium.

(g) The thickness of Al- and O-rich glassy films at Si/SiC grain boundaries was estimated to be around 1·5 nm after pressureless sintering.

Acknowledgements

Fruitful discussions were held with K. Rundgren from the Swedish Ceramic Institute and K. Ishizaki from Nagaoka University of Technology. The experimental materials were supplied by the Swedish Ceramic Institute. Financial support was received from the National Board for Industrial and Technical Development and the Swedish Research Council for Engineering Sciences.

References

1. Alliegro, R. A., Coffin, L. B. and Tinklepaugh, J. R., Pressure-sintered silicon carbide. *J. Am. Ceram. Soc.*, 1956, **39**, 386.
2. Tanaka, H., Sintering of silicon carbide. In *Silicon Carbide Ceramics*, ed. S. Somiya and Y. Inomata. Elsevier Applied Science, London, 1991, pp. 213–238.
3. Lange, F. F., Hot-pressing behaviour of silicon carbide powders with additions of aluminium oxide. *J. Mater. Sci.*, 1975, **10**, 314–320.
4. Prochazka, S., The role of boron and carbon in the sintering of silicon carbide. In *Special Ceramics 6*, ed. P. Popper and F. Fiee. British Ceramic Research Association, Stoke-on-Trent, 1975, pp. 171–181.
5. Cutler, R. A. and Jackson, T. B., Liquid phase sintered silicon carbide. In *Proc. 3rd International Symposium on Ceramic Materials and Components for Engines*, ed. V. J. Tennery. American Ceramic Society, Westerville, OH, 1989, pp. 309–318.
6. Jackson, T. B., Hurford, A. C., Bruner, S. L. and Cutler, R. A., SiC ceramics with improved strength. In *Silicon Carbide '87*, ed. J. D. Cawley and C. E. Semler. American Ceramic Society, Westerville, OH, 1989, pp. 227–240.
7. Lewis, M. H. and Lumby, R. J., Nitrogen ceramics: Liquid phase sintering. *Powder Metallurgy*, 1983, **26**(2), 73–81.
8. Hampshire, S. and Jack, K. H., The kinetics of densification and phase transformation of nitrogen ceramics. In *Special Ceramics 7*, ed. D. Taylor and P. Popper. British Ceramic Research Association, Stoke-on-Trent, 1981, pp. 37–49.
9. Lange, F. F., Silicon nitride polyphase systems: Fabrication, microstructure and properties. *Int. Met. Rev.*, 1980, No. 1, 1–20.
10. Ziegler, G., Heinrich, J. and Wötting, G., Review: Relationships between processing, microstructure and properties of dense and reaction-bonded silicon nitride. *J. Mater. Sci.*, 1987, **22**, 3041–3086.
11. Knutson-Wedel, E. M., Falk, L. K. L., Björklund, H. and Ekström, T., Si_3N_4 ceramics formed by HIP using different oxide additions — Relations between microstructure and properties. *J. Mater. Sci.*, 1991, **26**, 5575–5584.
12. Kahlman, L., Rundgren, K., Lidén, E., Nyberg, B. and Carlström, E., Processing of liquid phase sintered SiC — Mechanical and wear properties. In *Third Euro Ceramics V.3*, ed. P. Duran and J. F. Fernandez. Faenza Editrice Ibérica S. L., Castellon de la Plana, 1993, pp. 477–482.
13. Lidén, E., Persson, M., Carlström, E. and Carlsson, R., Electrostatic adsorption of a colloidal sintering agent on silicon nitride particles. *J. Am. Ceram. Soc.*, 1991, **74**, 1335–1339.
14. Ness, J. N., Stobbs, W. M. and Page, T. F., A TEM Fresnel diffraction-based method for characterizing thin grain-boundary and interfacial films. *Phil. Mag. A*, 1986, **54**, 679–702.
15. Cinibulk, M. K., Kleebe, H.-J. and Rühle, M., Quantitative comparison of TEM techniques for determining

amorphous intergranular film thickness. *J. Am. Ceram. Soc.*, 1993, **76**, 426–432.
16. Aksay, I. A. and Pask, J. A., Stable and metastable equilibria in the system SiO_2–Al_2O_3. *J. Am. Ceram. Soc.*, 1975, **58**, 507–512.
17. Toropov, N. A., Bondar, I. A., Galakhov, F. J., Nikogosyan, X. S. and Vinigradova, N. V. Phase equilibria in the yttrium oxide–alumina system. *Izv. Akad. Nauk. SSSR. Khim.*, 1964, **7**, 1076.
18. Bondar, I. A. and Galakhov, F. J., Phase equilibria in the system Y_2O_3–Al_2O_3–SiO_2. *Izv. Akad. Nauk. SSSR. Khim.*, 1964, **7**, 1325.
19. Cordrey, L., Niesz, D. E. and Shanefield, J., Sintering of silicon carbide with rare-earth oxide additions. In *Sintering of Advanced Ceramics*, ed. C. A. Handwerker, J. E. Blendell and W. Kaysser. The American Ceramic Society, Inc. Westerville, Ohio, 1990, pp. 618–636.
20. Toropov, N. A. and Bondar, I. A., Silicates of the rare earth elements, communication 3. Phase diagram of the binary system yttrium oxide-silica. *Izv. Akad. Nauk. SSSR. Otd. Khim. Nouk.*, 1961, **4**, 544–550.
21. Falk, L. K. L., Engström, U. and Rundgren, K., Intergranular microstructure and oxidation behaviour of Si_3N_4 ceramics formed with Y_2O_3, Al_2O_3 and ZrO_2. In *Silicon Nitride Ceramics — Scientific and Technological Advances*, ed. I.-W. Chen, P. F. Becker, M. Mitomo, G. Petzow and T.-S. Yen. Materials Research Society, Pittsburg, Pennsylvania, 1993, pp. 323–328.
22. Clarke, D. R., On the equilibrium thickness of intergranular glass phases in ceramic materials. *J. Am. Ceram. Soc.*, 1987, **70**, 15–22.
23. Clarke, D. R., Shaw, T. M., Philipse, A. P. and Horn, R. G., Possible electrical double-layer contribution to the equilibrium thickness of intergranular glass films in polycrystalline ceramics. *J. Am. Ceram. Soc.*, 1993, **76**, 1201–1204.
24. Raj, R. and Lange, F. F., Crystallisation of small quantities of glass (or liquid) segregated in grain boundaries. *Acta Metallurgica*, 1981, **29**, 1993–2000.
25. Kessler, H., Kleebe, H.-J., Cannon, R. W. and Pompe, W., Influence of internal stresses on crystallization of intergranular phases in ceramics. *Acta Metall. Mater.*, 1992, **40**, 2233–2245.
26. Falk, L. K. L. and Dunlop, G. L., Crystallisation of the glassy phase in a Si_3N_4 material by post-sintering heat treatments. *J. Mater. Sci.*, 1987, **22**, 4369–4376.
27. Sigl, L. S. and Kleebe, H.-J., Core/rim structures of liquid-phase-sintered silicon carbide. *J. Am. Ceram. Soc.*, 1993, **76**, 773–776.
28. Ogbuji, L. U., Mitchell, T. E. and Heuer, A. H., The $\beta \rightarrow \alpha$ transformation in polycrystalline SiC: III, The thickening of α plates. *J. Am. Ceram. Soc.*, 1981, **64**, 99.
29. Negita, K., Effective sintering aids for silicon carbide ceramics: Reactivities for silicon carbide with various additives. *J. Am. Ceram. Soc.*, 1986, **69**, C-308–C-310.
30. Watari, K. and Ishizaki, K., Influence of gas pressure on HIP sintered silicon nitride and stability of carbon impurity. *J. Ceram. Soc. Jpn Inter.* Ed., 1988, **96**, 535–540.
31. Ishizaki, K., Phase diagrams under high total gas pressures — Ellingham diagrams for hot isostatic press processes. *Acta Metall. Mater.*, 1990, **38**, 2059–2066.